Available online at www.sciencedirect.com
SCIENCE DIRECT®
International Journal of Thermal Sciences 44 (2005) 521–530
International Journal of Thermal Sciences
www.elsevier.com/locate/ijts

A computational study of convection heat transfer to CO_2 at supercritical pressures in a vertical mini tube

S. He [a,*], Pei-Xue Jiang [b], Yi-Jun Xu [b], Run-Fu Shi [b], W.S. Kim [a], J.D. Jackson [c]

[a] *School of Engineering, The Robert Gordon University, Aberdeen, AB10 1FR, UK*
[b] *Department of Thermal Engineering, Tsinghua University, Beijing 100084, China*
[c] *School of Mechanical, Aerospace and Civil Engineering, The University of Manchester, Oxford Road, Manchester M13 9PL, UK*

Received 21 June 2004; received in revised form 16 November 2004; accepted 29 November 2004

Abstract

Computational simulations of experiments on turbulent convection heat transfer of carbon dioxide at supercritical pressures in a vertical tube of diameter 0.948 mm have been carried out using low-Reynolds number eddy viscosity turbulence models. The simulations were able to reproduce the general features exhibited in the experiments, although, in some cases, the details between the simulations and the experiments were very different. A better understanding of the problem has been developed based on the information generated by the simulations on the detailed flow and turbulence fields. It has been shown that for mini tubes such as the one used in the current study, the buoyancy effect is generally insignificant. However, heat transfer can still be significantly impaired as a result of flow acceleration when the heating is strong, which causes a reduction in turbulence production. Such an effect can be described in terms of the heating acceleration parameter Ω_1. This parameter correlates reasonably well the data from all the cases considered in the current study.

Keywords: Supercritical fluids; Mini tube; Convection; CFD modelling; Flow acceleration

1. Introduction

Convection heat transfer in vertical channels is an important mode of heat transfer that occurs in many engineering applications such as heat exchangers, boilers, nuclear reactors, cooling systems for electronic components, etc. Despite the relatively simple geometry involved, the problem can be extremely complex due to one or more of the following influences: (a) buoyancy forces resulting from non-uniform density distribution over the cross section of the channel; (b) non-uniformity of thermal properties; and (c) acceleration or deceleration of the flow due to the expansion or contraction of the fluid as a result of significant axial variations of bulk temperature under heating or cooling. The effectiveness of heat transfer can be significantly reduced under certain circumstances which may have significant impact on the safety and/or economics of the operation of some industry plant. As a classical heat transfer problem, much effort has been devoted to studying this over many decades, and still there are considerable on-going interests in it. A detailed review of the work in this area was carried out by Jackson et al. [1]. Examples of more recent studies include Mikielewicz et al. [2], Celata et al. [3], Behzadmehr et al. [4], Bae et al. [5] and Baek and Park [6].

The phenomenon can be further complicated when the working fluid operates at a supercritical pressure. Under such a condition, there will be no phase changes with the increase of temperature. However, thermal properties can still vary dramatically with a small change in temperature over certain temperature range. The temperature, at which such variations are most dramatic, is called the pseudo-critical temperature. This is demonstrated in Fig. 1, where the variations of a number of thermal properties of CO_2 with temperature around the pseudo-critical temperature at 9.5 MPa are

* Corresponding author. Tel.: 0044 1224 262351, Fax.: 0044 1224 262444.
E-mail address: s.he@rgu.ac.uk (S. He).

1290-0729/$ – see front matter
doi:10.1016/j.ijthermalsci.2004.11.003

Nomenclature

A	cross section area of a pipe	m^2	
Bo^*	buoyancy parameter, $= Gr^*/(Re^{3.425}Pr^{0.8})$		
c_p	specific heat capacity	$J{\cdot}kg^{-1}{\cdot}K^{-1}$	
D	pipe diameter	m	
Gr^*	Grashof number, $= \beta g D^4 q''_w/(\lambda\nu^2)$		
h	heat transfer coefficient, $q_w/(T_w - T_b)$	$W{\cdot}m^{-2}{\cdot}K^{-1}$	
k	turbulent kinetic energy	$m^2{\cdot}s^{-2}$	
$\dot{m}$	mass flow rate	$kg{\cdot}s^{-1}$	
Nu	Nusselt number, $= hD/\lambda$		
Nu_0	Nusselt number for constant property forced convection		
Pr	Prandtl number, $= \mu c_p/\lambda$		
q''_w	convective heat flux from the wall	$W{\cdot}m^{-2}$	
r	radial coordinate	m	
Re	Reynolds number, $= U_b D/\nu$		
T	temperature	°C	
U_b	bulk velocity	$m{\cdot}s^{-1}$	
U, V	velocity components in x-, r-directions	$m{\cdot}s^{-1}$	
x	axial distance from start of heating	m	
y	normal distance from inner wall	m	
y^+	non-dimensional distance from pipe wall, $y(\tau_w/\rho)^{1/2}/\nu$		

Greek letters

β	volume expansion coefficient	K^{-1}
ε	rate of dissipation of k	$m^2{\cdot}s^{-3}$
λ	thermal conductivity	$W{\cdot}m^{-1}{\cdot}K^{-1}$
μ	molecular viscosity	$kg{\cdot}m^{-1}{\cdot}s^{-1}$
μ_t	turbulent viscosity	$kg{\cdot}m^{-1}{\cdot}s^{-1}$
ν	kinematic viscosity, $= \mu/\rho$	$m^2{\cdot}s^{-1}$
ρ	density of fluid	$kg{\cdot}m^{-3}$
Ω_1, Ω_2	heating acceleration parameters	

Subscripts

0	inlet; forced convection
b	bulk
w	wall
pc	pseudo-critical

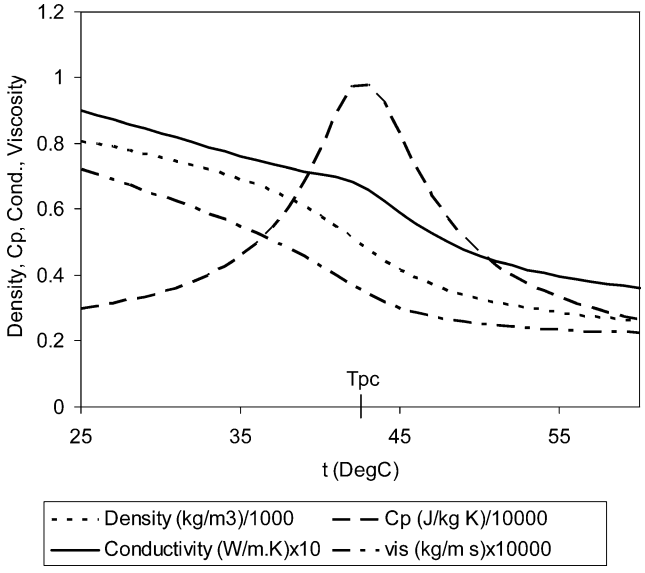

Fig. 1. Properties of CO_2 at 9.5 MPa.

shown. It can be seen clearly that the specific heat capacity can be doubled with a few degrees change in temperature. Other properties such as the thermal conductivity, viscosity and density, reduce significantly with the increase of temperature.

Research on heat transfer to fluids at supercritical pressures has been very active during the sixties driven by the introduction of conventional power plants working at supercritical pressure in order to improve the efficiency of these plants. Relatively fewer studies have been conducted since then. Recently, there has been a renewed interest in the topic driven by the active consideration of using fluids at supercritical pressure in a number of new applications, such as: waste processing, innovative air-conditioning systems, spacecraft cooling and the development of water-cooled nuclear reactors.

There has been an increasing interest recently in studies of heat transfer to fluids at supercritical pressures in mini/micro channels in connection with the development of innovative mini or compact gas coolers and internal heat exchangers for CO_2 high pressure trans-critical compression cycles in air-conditioners and heat pumps. CO_2, as an environmentally benign refrigerant, has been actively considered in a number of systems to substitute the environmental unfriendly refrigerants such as R12, R134a, etc. Examples of studies in this area include Jiang et al. [7] and Liao and Zhao [8].

A research program on turbulent convection heat transfer to CO_2 at supercritical pressure in vertical tubes of various diameters is being conducted aiming at developing a better understanding of the problem, which consists of a series of experimental, analytical and computational studies. The experimental study has been reported previously in Jiang et al. [9]. The current paper deals with the computational study. The aim of the computational study is twofold: (a) to evaluate the ability of turbulence models in simulating heat transfer to supercritical fluids in mini tubes, and (b) to assist with the understanding of the experimentally observed phenomena by providing detailed information on the flow and turbulence fields. The current study is one of the first computational studies which consider cases where the fluid temperature varies from below the pseudo-critical tempera-

ture to above it. Particular care needs to be taken to ensure the sharp variation of properties to be properly resolved.

2. Numerical modelling

The computational study has been conducted using an 'in-house' CFD code named SWIRL. It solves the transport equations for both the mean flow and turbulence in a cylindrical coordinator system using a widely used finite volume scheme (Patankar [10]). The flow is considered to be axisymmetric, and the Reynolds averaged equations for such a flow written in cylindrical coordinates are:

Continuity:

$$\frac{1}{r}\left\{\frac{\partial}{\partial x}(\rho r U)+\frac{\partial}{\partial r}(\rho r V)\right\}=0 \tag{1}$$

U-momentum:

$$\begin{aligned}&\frac{1}{r}\left\{\frac{\partial}{\partial x}\left(\rho r U^2\right)+\frac{\partial}{\partial r}(\rho r V U)\right\}\\&\quad=-\frac{\partial p}{\partial x}+\rho g+\frac{1}{r}\left\{2\frac{\partial}{\partial x}\left[r\mu_e\left(\frac{\partial U}{\partial x}\right)\right]\right.\\&\qquad\left.+\frac{\partial}{\partial r}\left[r\mu_e\left(\frac{\partial U}{\partial r}+\frac{\partial V}{\partial x}\right)\right]\right\}\end{aligned} \tag{2}$$

V-momentum:

$$\begin{aligned}&\frac{1}{r}\left\{\frac{\partial}{\partial x}(\rho r U V)+\frac{\partial}{\partial r}\left(\rho r V^2\right)\right\}\\&\quad=-\frac{\partial p}{\partial r}+\frac{1}{r}\left\{\frac{\partial}{\partial x}\left[r\mu_e\left(\frac{\partial V}{\partial x}+\frac{\partial U}{\partial r}\right)\right]\right.\\&\qquad\left.+2\frac{\partial}{\partial r}\left[r\mu_e\left(\frac{\partial V}{\partial r}\right)\right]\right\}-2\frac{\mu_e V}{r^2}\end{aligned} \tag{3}$$

in which μ_e is the effective viscosity defined by $\mu_e=\mu+\mu_T$ in which μ_T is the turbulent viscosity and ρ is the density.

The energy equation for the case where there are variations of properties with temperature is:

Energy equation:

$$\begin{aligned}&\frac{1}{r}\left\{\frac{\partial}{\partial x}(\rho C_p r U T)+\frac{\partial}{\partial r}(\rho C_p r V T)\right\}\\&\quad=\frac{1}{r}\left\{\frac{\partial}{\partial x}\left[rC_p\left(\frac{\mu}{Pr}+\frac{\mu_t}{\sigma_T}\right)\frac{\partial T}{\partial x}\right]\right.\\&\qquad\left.+\frac{\partial}{\partial r}\left[rC_p\left(\frac{\mu}{Pr}+\frac{\mu_t}{\sigma_T}\right)\frac{\partial T}{\partial r}\right]\right\}\end{aligned} \tag{4}$$

in which Pr is the molecular Prandtl number and σ_T the turbulent Prandtl number.

As far as the modelling of turbulent diffusion is concerned, since the flow in question can be strongly distorted in comparison with 'conventional' wall shear flows due to influences of buoyancy and non-uniformity of fluid properties, the use of the standard k–ε turbulence model coupled with a simple wall function (the latter is used in the region near the wall) is not appropriate. Low–Reynolds number (LRN) turbulence models, which extend the standard model by including the modelling of the effects of the wall and the molecular diffusion, can be used in the wall region as well as the core, and are therefore potentially more suitable. A number of LRN k–ε models have been used in a preliminary study of the current investigation. These included those due to Launder and Sharma (LS) [11], Chien (CH) [12], Lam and Bremhorst (LB) [13] and Abe, Kondoh and Nagano (AKN) [14]. All these models were able to reproduce the general trend. Yet models due to Launder–Sharma and Chien appeared to perform marginally better than others in the tests conducted. Taking into account the fact that these two models also performed better in an earlier study on convection heat transfer to supercritical fluids in normal sized tubes (He et al. [15]), the main study was carried out using the LS and CH models. The overall performance of the two models was similar, and the discussion will be mainly based on the simulations using the LS model.

The constitutive and transport equations of the LS k–ε model [11] can be written as:

Constitutive equation:

$$\mu_t=C_\mu f_\mu \rho k^2/\varepsilon \tag{5}$$

k-transport equation:

$$\begin{aligned}&\left[\frac{\partial(\rho U k)}{\partial x}+\frac{1}{r}\frac{\partial(r\rho V k)}{\partial r}\right]\\&\quad=\frac{\partial}{\partial x}\left[\left(\mu+\frac{\mu_t}{\sigma_k}\right)\frac{\partial k}{\partial x}\right]+\frac{1}{r}\frac{\partial}{\partial r}\left[r\left(\mu+\frac{\mu_t}{\sigma_k}\right)\frac{\partial k}{\partial r}\right]\\&\qquad+P_k+G_k-\rho(\tilde{\varepsilon}+D)\end{aligned} \tag{6}$$

in which

$$\begin{aligned}P_k=\mu_t\Bigg[&2\left\{\left(\frac{\partial U}{\partial x}\right)^2+\left(\frac{\partial V}{\partial r}\right)^2+\left(\frac{V}{r}\right)^2\right\}\\&+\left(\frac{\partial U}{\partial r}+\frac{\partial V}{\partial x}\right)^2\Bigg]\end{aligned} \tag{7}$$

(shear production)

$$\begin{aligned}G_k&=-\overline{\rho' u'}g_x\\&=-\frac{\beta\mu_t}{C_{1t}}\left(\frac{k}{\varepsilon}\right)\left(\frac{\partial U}{\partial r}+\frac{\partial V}{\partial x}\right)\left(\frac{\partial T}{\partial r}\right)g_x\end{aligned} \tag{8}$$

(gravitational production)

$\tilde{\varepsilon}$-transport equation:

$$\begin{aligned}&\left[\frac{\partial(\rho U\tilde{\varepsilon})}{\partial x}+\frac{1}{r}\frac{\partial(r\rho V\tilde{\varepsilon})}{\partial r}\right]\\&\quad=\frac{\partial}{\partial x}\left[\left(\mu+\frac{\mu_t}{\sigma_\varepsilon}\right)\frac{\partial\tilde{\varepsilon}}{\partial x}\right]+\frac{1}{r}\frac{\partial}{\partial r}\left[r\left(\mu+\frac{\mu_t}{\sigma_\varepsilon}\right)\frac{\partial\tilde{\varepsilon}}{\partial r}\right]\\&\qquad+C_{\varepsilon1}\frac{\tilde{\varepsilon}}{k}(P_k+G_k)-C_{\varepsilon2}f_2\frac{\rho\tilde{\varepsilon}^2}{k}+\rho E\end{aligned} \tag{9}$$

and the model constants and damping functions are:

$$C_\mu = 0.09, \qquad C_{\varepsilon 1} = 1.44, \qquad C_{\varepsilon 2} = 1.92$$

$$C_{1t} = 3.2, \qquad \sigma_k = 1.0, \qquad \sigma_\varepsilon = 1.3, \qquad \sigma_T = 0.9$$

$$f_\mu = \exp\left[\frac{-3.4}{(1+Re_t/50)^2}\right], \qquad f_2 = 1 - 0.3\exp\left(-Re_t^2\right)$$

$$D = 2\nu\left[\left(\frac{\partial\sqrt{k}}{\partial x}\right)^2 + \left(\frac{\partial\sqrt{k}}{\partial r}\right)^2\right] \quad \text{and}$$

$$E = 2\nu\nu_t\left[\left(\frac{\partial^2 U}{\partial x^2}\right)^2 + \left(\frac{\partial^2 U}{\partial r^2}\right)^2 + 2\left(\frac{\partial^2 U}{\partial x\,\partial r}\right)^2 + \left(\frac{\partial^2 V}{\partial x^2}\right)^2 + \left(\frac{\partial^2 V}{\partial r^2}\right)^2 + 2\left(\frac{\partial^2 V}{\partial x\,\partial r}\right)^2\right],$$

where $\nu_t = \mu_t/\rho$, $Re_t = \frac{k^2}{\nu\tilde{\varepsilon}}$ and $\tilde{\varepsilon} = \varepsilon - D$.

The complete computational domain, which covered the whole heated length of the test section and over 20 diameter length of the pre-heated section and ranged from the centre of the tube to the inner wall, was discretized into a mesh of grids, typically, 92 × 62 (axial × radial). The mesh was refined in the radial direction towards the tube wall. The mesh was adjusted in each individual run to ensure that the near-wall flow features were properly resolved. The y^+ value at the first node of the mesh was always less than 0.5. The mesh was also refined in the axial direction towards the region where the heating commenced.

The staggered grid arrangement was used to define the variables. The scalar parameters were defined at the grid points and the velocity components were defined on the control volume surfaces. The QUICK scheme was used for approximating the convection terms in the momentum equations. This ensured relatively good accuracy. The UPWIND scheme was used for other transport equations for reasons of numerical stability. The SIMPLE scheme was used for coupling the pressure and the velocity fields. The resulting five-point coefficient matrix system was solved iteratively using the line-by-line TDMA algorithm: at any time, variables at a particular line were solved simultaneously; variables at the neighbouring lines were assumed to be known and values from the previous iteration were used.

The NIST Standard Reference Database 23 (REFPROP) Version 7 was used for calculating the temperature (and pressure) dependent properties of carbon dioxide. To do this, the relevant FORTRAN subroutines supplied with the Database were incorporated in the CFD code SWIRL.

The CFD code employed has been previously used and validated in a number of studies (He et al. [15,16]). The uncertainty of the numerical methods used was assessed in this study in terms of the mesh dependency and convergence criteria. The size of the radial mesh was considered to be essential and the number of radial mesh was doubled to 122 in a test. The difference between the maximum wall temperature ($T_{w\max}$) in this and the standard run (a mesh of 62) was about 0.5% of the range of fluid temperature. The stop criterion for iteration was based on averaged relative residuals of the transport equations and a value of 0.5×10^{-6} was used. Reducing this value by a magnitude caused the $T_{w\max}$ to change by less than 1% of the fluid temperature range.

3. Computational results and comparison with experimental data

3.1. The experiments simulated

The experiments simulated in the current study were carried out in a vertical tube of stainless steel 1Cr18N9T of internal and external diameters of 0.948 and 1.729 mm respectively, and a heated length of 0.055 m, see Fig. 2. Pressurised CO_2 was used as the working fluid which was held at a nominal supercritical pressure of 8.5 or 9.5 MPa. The test section was directly heated by passing a low voltage al-

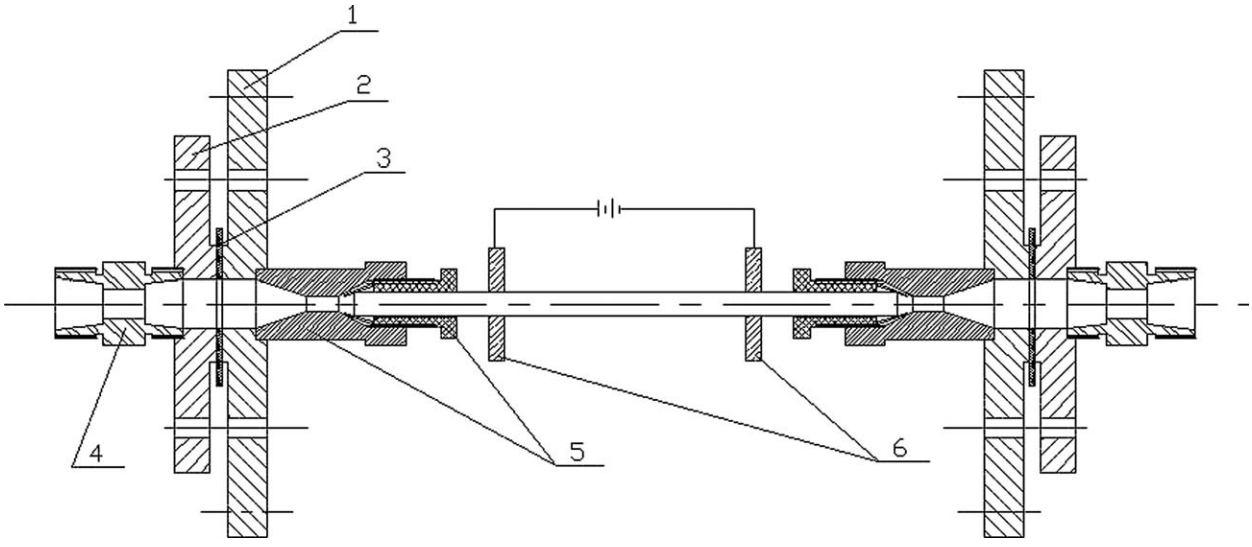

Fig. 2. Test section geometry: 1 square flange; 2 circular flange; 3 polytetrafluoroethylene spacer (PTFE); 4, 5 connecting fittings; 6 copper electrode. (Reproduced from Jiang et al. [9].)

Table 1
Experimental conditions of tests simulated

Test ID	m [kg·h^{-1}]	T_0 [°C]	P_0 [MPa]	Re_0	Bo_0^*	q''_w [W·m^{-2}]	Ω_1	Ω_2
P01LS	1.48	32.7	9.59	9237	9.36E–08	31534	1.13E–03	1.12E–07
P02LS	1.53	37.8	9.54	11639	7.9E–08	31194	1.34E–03	1.05E–07
P03LS	1.49	39.6	9.5	12629	7.96E–08	30722	1.47E–03	1.06E–07
P04LS	1.37	51	9.43	20864	2.08E–08	29400	1.48E–03	6.81E–08
P11LS	1.69	32.8	9.52	10641	1.36E–07	71843	2.52E–03	1.99E–07
P12LS	1.6	36.1	9.42	11474	1.61E–07	71703	3.07E–03	2.2E–07
P13LS	1.63	40.9	9.57	14765	1.24E–07	70242	3.26E–03	1.83E–07
P14LS	1.65	48.3	9.49	23417	3.67E–08	70005	2.95E–03	1.14E–07
P21LS	1.48	32.7	9.59	9237	9.36E–08	31534	1.13E–03	1.12E–07
P22LS	1.71	32.7	9.49	10761	7.19E–08	39554	1.25E–03	1.06E–07
P23LS	2.93	33.4	9.47	18888	1.31E–08	45561	8.37E–04	4.15E–08
P24LS	3.45	31.7	9.55	20972	6.21E–09	37744	5.31E–04	2.42E–08
P25LS	4.17	31	9.56	24837	3.4E–09	39558	4.46E–04	1.73E–08
P41LS	4.06	33.4	8.57	29255	3.75E–09	37700	5.87E–04	1.92E–08
P42LS	4.03	33.4	8.47	29585	6.86E–09	66583	1.12E–03	3.49E–08
P43LS	4.08	33.3	8.51	29558	9.92E–09	100770	1.70E–03	5.12E–08
P44LS	4.08	33.3	8.51	29558	1.97E–08	200000	3.74E–03	1.01E–07
P45LS	4.06	33.4	8.57	29255	9.96E–10	10000	1.49E–04	5.04E–09
P51LS	1.51	33.5	8.46	11173	1.16E–07	38993	1.85E–03	1.46E–07
P52LS	1.52	35	8.46	12537	1.1E–07	38692	1.97E–03	1.39E–07
P53LS	1.5	38.4	8.47	19379	4.67E–08	36287	1.97E–03	9.32E–08
P54LS	1.49	44	8.48	24138	1.74E–08	37079	1.78E–03	7.05E–08

Note: Ω_1 & Ω_2 were evaluated at $x/D = 50$, to be consistent with data presented in Figs. 5–8.

ternating current electricity through it. The measurements included the wall temperatures, inlet and outlet fluid temperatures, the inlet pressure and pressure drop across the test section, the flow rate and the power input to the heated test section. In particular, the temperature at the outer wall of the test section was measured using a number of thermocouples welded on its surface. The temperature on the inner surface was then derived using a one-dimensional numerical analysis. The experimental uncertainties, in terms of the root mean square variations of the convective heat transfer coefficient, were estimated to be 11.3% [9]. Further information on the experimental arrangement can be found in Jiang et al. [9]. The experimental conditions of the tests which have been simulated in this study are shown in Table 1.

3.2. Comparison of predicted wall temperatures with experimental measurements

Figs. 3(a)–(c) show comparisons of the wall temperatures obtained from the simulations using the LS turbulence model with those measured from the experiment for cases with various inlet fluid temperatures. Other experimental conditions, including the mass flow rate, heat input and the pressure at the inlet, were maintained approximately the same for the various cases in each figure. A dashed line is also shown in each figure to indicate the approximate value of pseudo-critical temperature (T_{pc}). Strictly speaking T_{pc} is different in each run. The bulk temperatures (T_b) from the simulations are also shown.

As the thermal properties of supercritical fluids vary sharply around the pseudo-critical temperature, it is clearly useful to classify the tests with respect to if the temperature of the fluid in a test goes through the pseudo-critical temperature (T_{pc}) or not. For the convenience of discussion, we will regard a convection heat transfer to supercritical fluid test as a regime I case, if the bulk and the wall temperatures are all below T_{pc}; regime II case if all are above T_{pc}; or regime III case if the bulk temperature is below T_{pc} but the wall temperature is above it.

Two regime III, one regime I and one regime II test cases are shown in Fig. 3(a). For this series of tests, the pressure was kept at a nominal value of 9.5 Mpa and imposed heat flux was relatively low, at ∼30 kW·m^{-2}. It can be seen from the figure that the wall temperatures obtained from the simulations are all very close to the measurements. This is particularly true for the two regime III cases. The heat flux was increased to ∼70 kW·m^{-2} in the tests shown in Fig. 3(b). Two of the cases can be classified as regime IIs and two regime IIIs. Again the simulation results are fairly close to the measurements apart from in the case of run P12 (a regime III case), where the predicted wall temperature by the modelling is significantly higher than the experimental data.

For cases shown in Fig. 3(c) the heat flux (∼37 kW·m^{-2}) was comparable to that of the cases shown in Fig. 3(a) but the pressure was reduced to around 8.5 MPa. As a result, the variation of thermal properties around the pseudo-critical temperature was stronger. It is interesting to note that the simulations for the two regime III cases are fairly close to the experiments. The predictions of the wall temperature for the two regime II cases are, on the other hand, significantly lower than the measurements.

Fig. 3(d) shows wall temperatures predicted by simulations using LS model for cases of various mass flow rates.

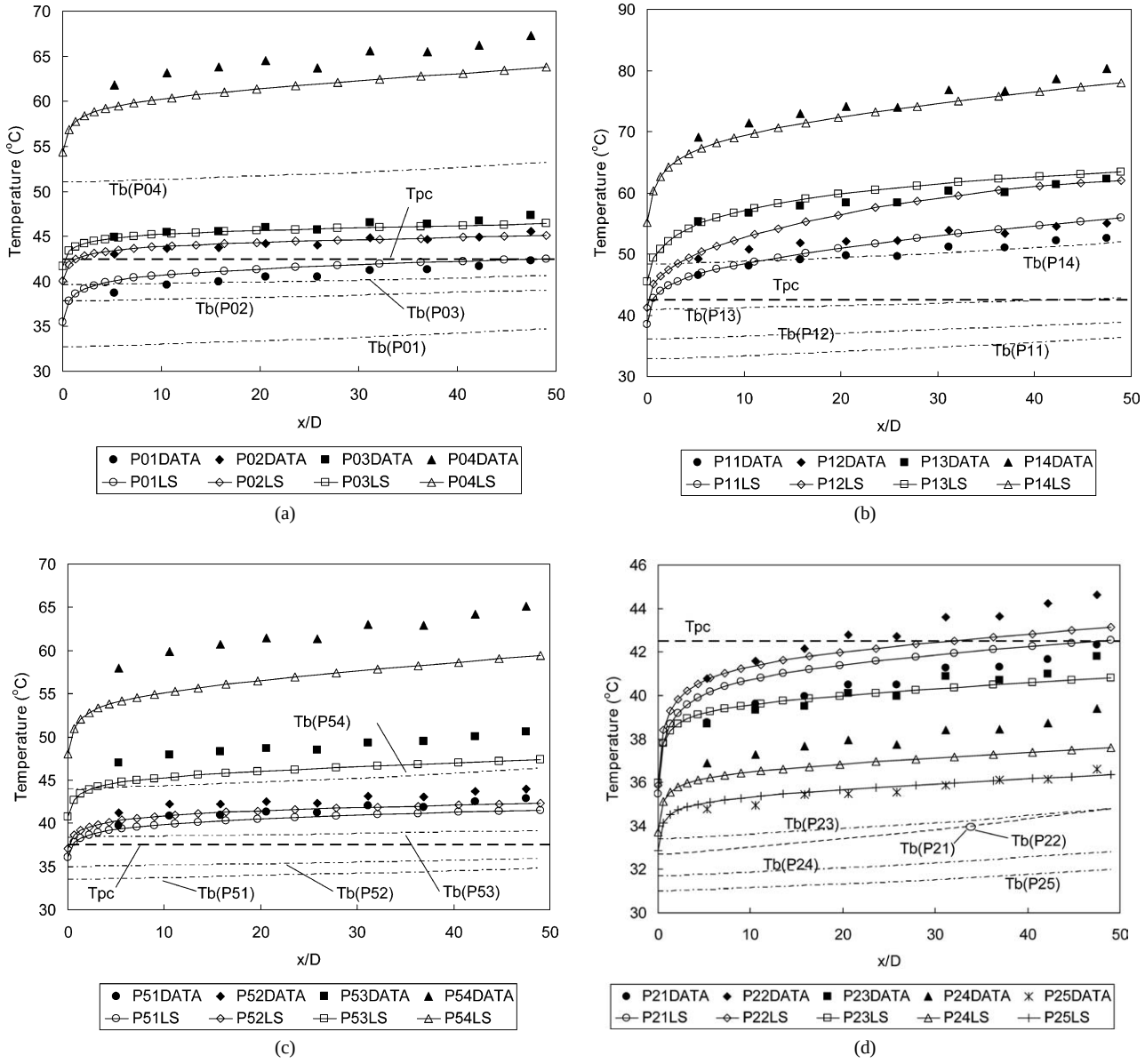

Fig. 3. Axial variations of wall and bulk temperatures. (a) Series 01 (nominal conditions: $\dot{m} = 1.5$ kg·h^{-1}, $P_0 = 9.5$ Mpa, $q''_w = 30$ kW·m^{-2}); (b) Series 10 (nominal conditions: $\dot{m} = 1.6$ kg·h^{-1}, $P_0 = 9.5$ Mpa, $q''_w = 70$ kW·m^{-2}); (c) Series 50 (nominal conditions: $\dot{m} = 1.5$ kg·h^{-1}, $P_0 = 8.5$ Mpa, $q''_w = 37$ kW·m^{-2}); (d) Series 20 (nominal conditions: $T_0 = 32\,^{\circ}$C, $P_0 = 9.5$ Mpa, $q''_w = 40$ kW·m^{-2}).

Other conditions including the pressure and temperature at inlet and the heat flux were kept fairly similar. The predictions agree extremely well with experiments in cases P23 and P25. For other cases, some discrepancies between the predictions and the experimental data are shown, although none is significant.

Herwig and Hausner [17] showed that for a laminar flow in a minichannel, conduction through the tube wall may contribute significantly to the so-called 'micro-effect'. A calculation including the conduction in the tube wall was done to evaluate such an effect. The effect on wall temperature was found to be reasonably small for the current turbulent flow cases in regions away from the first five diameters downstream of the starting point of heating.

3.3. Comparison of predicted heat transfer coefficients with those obtained from measurements

Fig. 4 shows comparisons of the heat transfer coefficients calculated from the simulations using the LS model with those measured from the experiments for the cases corresponding to these shown in Fig. 3(a). The general trend of the effect of varying the inlet temperature on the heat transfer coefficient (htc) shown in the experimental data has been reproduced by the simulations. But the discrepancies between the predictions and the measurements appear to be generally larger in the case of htc than in wall temperature. Some of these are due to the differences between the measured and the predicted bulk temperature, which could be quite large in

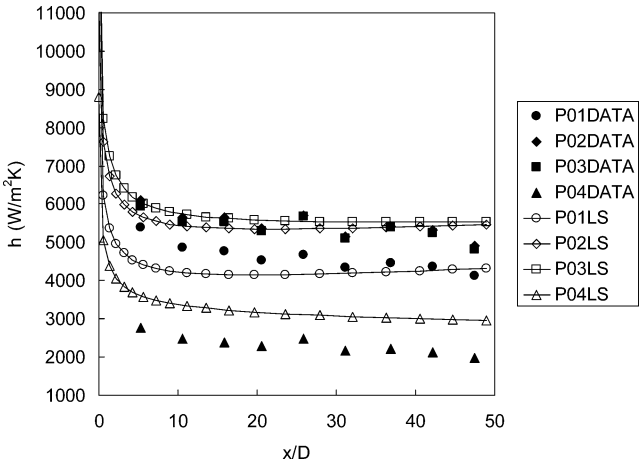

Fig. 4. Heat transfer coefficient variations in series 01 (nominal conditions: $\dot{m} = 1.5$ kg·h^{-1}, $P_0 = 9.5$ Mpa, $q''_w = 30$ kW·m^{-2}).

cases when the local variation of properties was very sharp. A major source for such inconsistencies was found to stem from the differences between the thermal property data used in the modelling (NIST REFPROP version 7) and experimental studies (NIST REFPROP version 6).

4. Discussion

4.1. Effect of buoyancy

The buoyancy parameter, $Bo^* = Gr^*/(Re^{3.425}Pr^{0.8})$, introduced by Jackson and Hall [18] can be used to estimate the influences of buoyancy on heat transfer. The value of this buoyancy parameter has been calculated for each test case and is shown in Table 1 together with other parameters. The criterion for the buoyancy effect to be significant has been suggested to be greater than $\sim 5.6 \times 10^{-7}$ (Mikielewicz et al. [2]). Clearly for all the experiments considered in the current study, the buoyancy parameter is far below this criterion. Care should however be taken when such an approach is used in situations involving supercritical fluids since the buoyancy parameter is normally estimated using the thermal properties based on the bulk temperature. But near the T_{pc}, thermal properties may vary sharply and the buoyancy parameter based on the bulk temperature may not be very representative in some extreme situations.

In order to investigate the effect of buoyancy, sensitivity studies have been carried out for a number of cases. Simulations with the buoyancy term removed have been conducted together with normal runs (with the usual buoyancy terms). It has been found that for all cases tested the buoyancy effects were insignificant. Therefore it can be concluded that for mini tubes such as the one used in the current study, the buoyancy effect is normally always low even when the heating is relatively strong. The mode of heat transfer can be considered as forced convection.

4.2. Effects of heat flux and flow acceleration

The review article by Jackson [19] discussed the influences of heat flux in forced convection heat transfer to supercritical fluids. Depending on the strength of the heating, the effectiveness of heat transfer can be enhanced or impaired, as a result of the balance of two effects: the effects of the sharp variation of thermal properties and the effect of flow acceleration due to heating. At a low heat flux condition, heat transfer has been found to be enhanced. With the increase of heat flux, the enhancement will reduce until a stage where heat transfer is impaired. The explanation offered in Jackson [19] is briefly outlined below with reference to a regime III case, where the bulk temperature is below the T_{pc} and the wall temperature above it.

It can be seen from Fig. 1 that near the pseudo-critical temperature, due to an increase of temperature near the wall, the viscosity and thermal conductivity will decrease, and the specific capacity (c_p) will increase significantly. The decrease of the thermal conductivity will cause a decrease in heat transfer. But the decrease in viscosity will cause the viscous sub-layer to become thinner and therefore an enhancement in heat transfer. The increase of c_p will also cause a heat transfer enhancement due to an increased convection capacity—for the same mass flow, more heat is removed. Experimental data clearly show that for a case of low heat flux, the latter two overweigh the first effect and overall, heat transfer is enhanced.

With the increase of heat flux and therefore a large bulk to wall temperature difference, the high value of c_p near T_{pc} is felt within a limited region and therefore its effect reduces. Consequently, the heat transfer enhancement is reduced. Consider another effect of variable property which is related to the density changes. With the increase of bulk temperature, the density decreases and, due to the increased volume, the flow is accelerated. This causes the turbulence production to reduce and heat transfer deteriorated. When the heat flux is low, such an effect is small. But at very high heat flux, turbulence may be significantly reduced and the flow may even be re-laminarised. This effect dominates cases of high heat fluxes and causes an overall heat transfer deterioration.

The effect of increasing heat flux was investigated in both the experimental and computational studies. Fig. 5 shows the local heat transfer coefficient (htc) at the section $x/D = 50$, towards the end of the heated section, therefore free from the entrance effect. Both experimental data and computational results are presented. The latter also include two extra runs (P44 & P45), one with a higher heat flux (200 kW·m^{-2}) and one with a lower one (10 kW·m^{-2}) to cover wider conditions. The predictions are significantly higher than the experimental data. However, the trend of the variation of the experimental data appears to be reproduced by the simulations. Initially with the increase of heat flux, the htc increases. This is thought to be caused by the effect of the variation of thermal properties, which is consistent with that found in normal

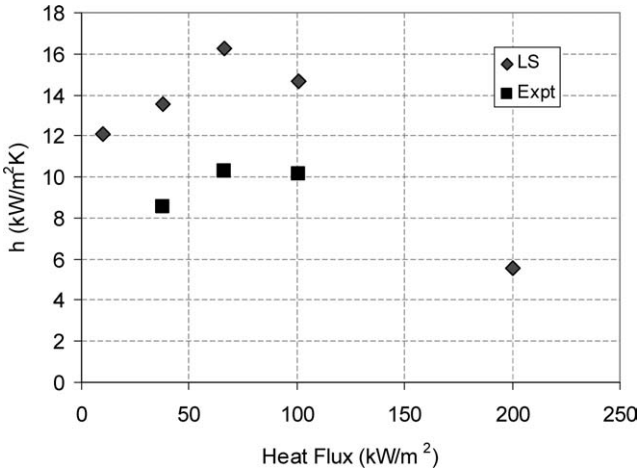

Fig. 5. Heat transfer coefficient as a function of heat flux (series 40) (nominal conditions: $\dot{m} = 4\ \mathrm{kg{\cdot}h^{-1}}$, $P_0 = 8.5$ Mpa, $T_0 = 33\,^{\circ}\mathrm{C}$).

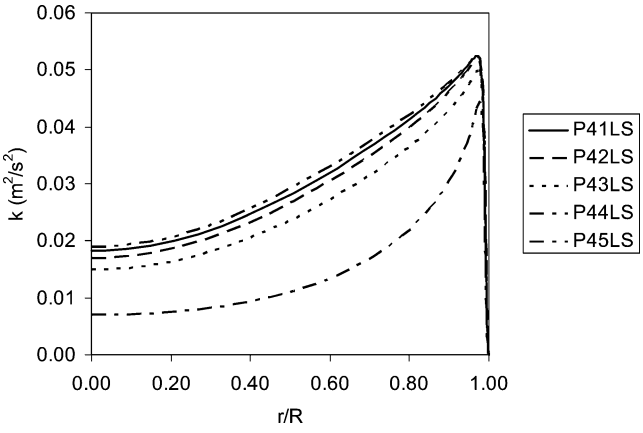

Fig. 6. Profiles of turbulence kinetic energy at $x/D = 50$ (series 40) (nominal conditions: $\dot{m} = 4\ \mathrm{kg{\cdot}h^{-1}}$, $P_0 = 8.5$ Mpa, $T_0 = 33\,^{\circ}\mathrm{C}$).

sized tubes as explained by Jackson [19] and above. When the heat flux is high, the htc is significantly reduced due to the flow acceleration, again consistent with earlier observations.

The profiles of turbulence kinetic energy (k) at section $x/D = 50$ are shown in Fig. 6. Initially, with the increase of heat flux, the k reduces slightly. This clearly has insignificantly effect on heat transfer which is mostly influenced by thermal property variations. For case P44, where the heat flux is very strong ($200\ \mathrm{kW{\cdot}m^{-2}}$), however, k is significantly reduced, which is clearly responsible for the reduction of htc shown in Fig. 5 above.

In order to investigate the effect of the variation of an individual property with temperature, sensitivity runs were carried out, where one or more properties were kept constant while others were allowed to vary as normal. Fig. 7 shows results from a number of tests, based on P44, especially looking at the effect of the variation of density versus these of other thermal properties. The results are shown as

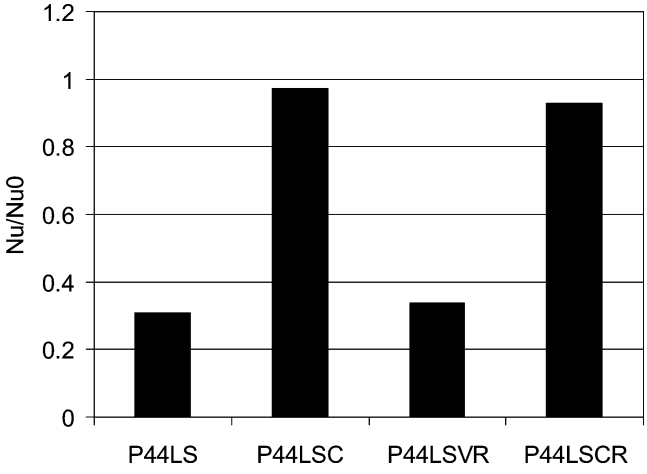

Fig. 7. Effect of variations of fluid density (P44LS: full model; P44LSC: all = const.; P44LSVR: variable ρ only, other properties = const; P44LSCR: ρ = const & others vary normally).

the Nusselt number (Nu) normalised using that calculated from a correlation for constant property forced convection:

$$Nu_0 = 0.023 Re^{0.8} Pr^{0.4} \tag{10}$$

The properties were evaluated based on the bulk temperature. It can be seen from the figure that the Nu ratio is close to unity for the constant property calculation (P44LSC) as expected. The Nu ratio reduces to about 0.3 for the calculation using the full model (P44LS), indicating severe heat transfer deterioration. When all thermal properties were fixed at a constant except for the density which was allowed to vary with temperature as normal (P44LSVR), the Nu ratio obtained was very similar to that for the full model. However, when the density was fixed at a constant and other properties were allowed to vary as normal, the Nu ratio was close to unity. These results clearly suggest that it was the variation of density which was principally responsible for the reduction in heat transfer and the combined effect of the variation of other properties appear to be small in this particular case. The reduction of density causes flow acceleration which results in a velocity profile impairing the turbulence production. For example, the turbulent viscosity in the full model was only about a third of that in the constant property simulation in the near wall region.

4.3. Correlation of data using acceleration parameters

Non-dimensional parameters can be derived to describe the effect of flow acceleration due to heating. Consider the velocity acceleration in a flow of a mass flow rate $\dot{m}$, heated by a heat flux q''_w. The acceleration can be represented by $\mathrm{d}U_b/\mathrm{d}x$. That is,

$$\frac{\mathrm{d}U_b}{\mathrm{d}x} = \frac{\mathrm{d}(\dot{m}/\rho A)}{\mathrm{d}x} \tag{11}$$

Therefore

$$\frac{\mathrm{d}U_b}{\mathrm{d}x} = \frac{\dot{m}}{\rho A}\left(-\frac{1}{\rho}\frac{\mathrm{d}\rho}{\mathrm{d}T}\right)\frac{\mathrm{d}T}{\mathrm{d}x} \tag{12}$$

Considering the energy balance in a short section dx of the pipe, we have

$$\frac{\mathrm{d}T}{\mathrm{d}x} = \frac{q''_w \pi D}{\dot{m} C_p} \tag{13}$$

Combining Eqs. (12) and (13), and also considering that $-\frac{1}{\rho}\frac{\mathrm{d}\rho}{\mathrm{d}T}$ is the volume expansion coefficient represented by β yields:

$$\frac{\mathrm{d}U_b}{\mathrm{d}x} = \frac{4\beta q''_w}{\rho C_p D} \tag{14}$$

Two types of parameters can be considered to be used to normalise the acceleration: a parameter based on the 'outer' scale, U_b/D or one based on the 'inner' scale, ν/U_b^2. It follows, when the outer scale U_b/D is used,

$$\Omega_1 = \frac{\mathrm{d}U_b}{\mathrm{d}x}\frac{D}{U_b} = \frac{4\beta q''_w}{\rho C_p U_b} \tag{15}$$

Or, when the inner scale ν/U_b^2 is used,

$$\Omega_2 = \frac{\mathrm{d}U_b}{\mathrm{d}x}\frac{\nu}{U_b^2} = \frac{4\beta q''_w \nu}{\rho C_p D U_b^2} \tag{16}$$

The above parameters will be referred to as heating acceleration parameters Ω_1 and Ω_2 respectively hereafter. They are related to each other through:

$$\Omega_2 = \frac{4\beta q''_w \nu}{\rho C_p D U_b^2} = \frac{4\beta q''_w}{\rho C_p U_b}\frac{\nu}{D U_b} = \frac{\Omega_1}{Re} \tag{17}$$

The Ω_1 is simply 4 times the non-dimensional heat rate q^+ used by Bankston and McEligot [20] and Mikielewicz et al. [2], which was obtained from non-dimensionalizing the governing equations and boundary conditions in pipe flow with an imposed heat flux distribution. The Ω_2 is actually in the exact form as K_ν used by Kline et al. [21] for describing effect of flow acceleration in external boundary layers, when the free stream velocity in K_ν is replaced with the bulk velocity. The reader is referred to McEligot et al. [22] for more discussion.

Fig. 8 shows the ratios of the Nusselt number predicted by the modelling over that calculated using the correlation for constant property forced convection (Eq. (10)) as a function of the heating acceleration parameter Ω_1 and Ω_2 respectively for all the cases considered in this study. It is clear that there is a well defined trend in Fig. 8(a) but not in Fig. 8(b), which suggests that Ω_1 is a suitable parameter which can be used to correlate the data from the current study. The level of heat transfer impairment increases with the increase of Ω_1. As discussed above in relation to Fig. 7, this is believed to be principally caused by flow acceleration due to heating.

The above results are not completely consistent with earlier studies such as McEligot et al. [22], in which the parameter K_ν ($= \Omega_2$) was found to be the most suitable parameter for evaluating flow accelerating effect. The acceleration effect in the current study would have been judged to be insignificant using their criterion. Some of these discrepancies

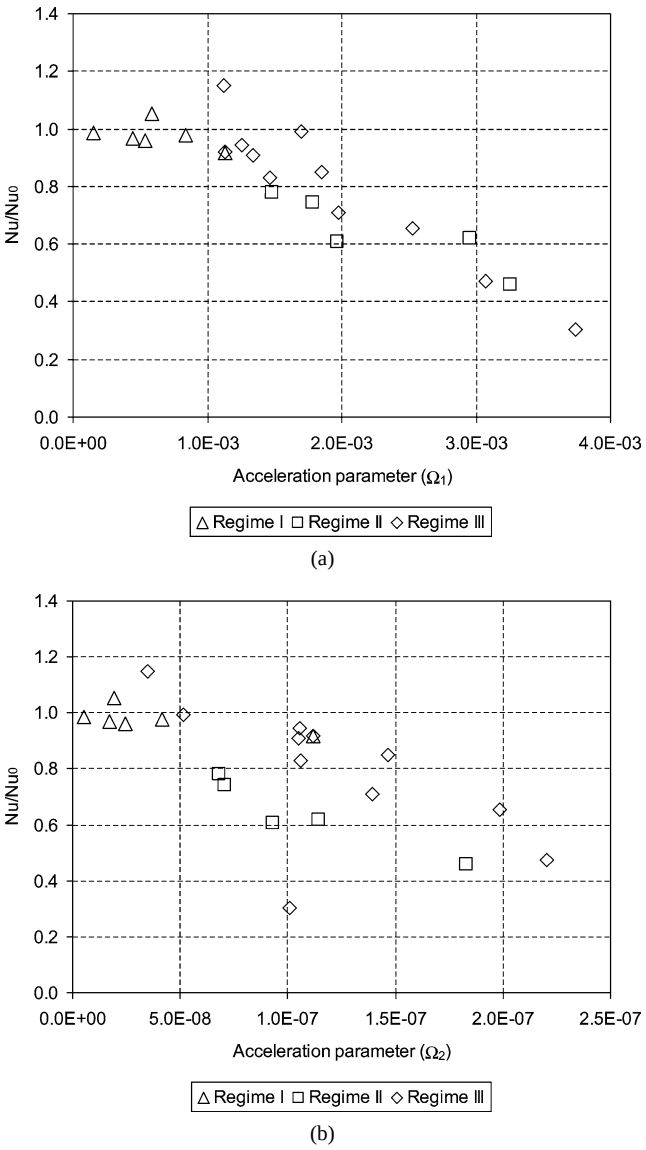

Fig. 8. Nusselt number ratio as a function of a heating acceleration parameter. (a) *Nu* ratio *versus* Ω_1; (b) *Nu* ratio *versus* Ω_2.

may be explained by the fact that, close to T_{pc}, thermal properties including density vary extremely sharply, which may not be well represented by the parameters evaluated at the bulk temperature.

5. Conclusions

The simulations using the low Reynolds number k–ε turbulence model due to Launder–Sharma has been found to be able to reproduce the general features exhibited in the experiments on convection heat transfer to CO_2 at supercritical pressures in a vertical mini tube. However, in some cases, the details of the simulation results can be very different from the experimental data. The modelling study provided valuable information on the detailed flow and turbulence fields, which has been used in the development of a better under-

standing of the physical problem. It has been shown that for mini tubes such as the one used in the current study, the buoyancy effect is generally insignificant even when a relatively high heat flux is imposed. The heat transfer can be significantly impaired when the heating is strong and this is caused by the reduced turbulence induced by the flow acceleration which is in turn caused by a high heat flux. Such an effect can be described by the heating acceleration parameter Ω_1. This parameter correlates reasonably well the data from all the cases considered in the current study.

Acknowledgement

The project was undertaken under support from the EPSRC (GR/S19424/1), National Outstanding Youth Fund from the National Natural Science Foundation of China (No. 50025617) and the Royal Society (GF148NEZ).

References

[1] J.D. Jackson, M.A. Cotton, B.P. Axcell, Studies of mixed convection in vertical tubes, Internat. J. Heat Fluid Flow 10 (1989) 2–15.
[2] D.P. Mikielewicz, A.M. Shehata, J.D. Jackson, D.M. McEligot, Temperature, velocity and mean turbulence structure in strongly heated internal gas flows: Comparison of numerical predictions with data, Internat. J. Heat Mass Transfer 45 (2002) 4333–4352.
[3] G.P. Celata, F.D. Annibale, A. Chiaradia, M. Cumo, Up flow turbulent mixed convection heat transfer in vertical pipes, Internat. J. Heat Mass Transfer 41 (1998) 4037–4054.
[4] A. Behzadmehr, N. Galanis, A. Laneville, Low Reynolds number mixed convection in vertical tubes with uniform wall heat flux, Internat. J. Heat Mass Transfer 46 (2003) 4823–4833.
[5] J.H. Bae, J.Y. Yoo, H. Choi, Direct numerical simulation of heat transfer to CO_2 at supercritical pressure in a vertical tube, in: NURETH-10, Seoul, October 5–9, 2003.
[6] S.G. Baek, S.O. Park, Prediction of strongly-heated gas flows in a vertical tube using explicitly algebraic stress/heat-flux models, in: NURETH-10, Seoul, October 5–9, 2003.
[7] P.X. Jiang, B.X. Wang, D.A. Luo, Z.P. Ren, Fluid flow and convective heat transfer in a vertical porous annulus, Numer. Heat Transfer A 30 (1996) 305–320.
[8] S.M. Liao, T.S. Zhao, An experimental investigation of convection heat transfer to supercritical carbon dioxide in miniature tubes, Internat. J. Heat Mass Transfer 45 (2002) 5025–5034.
[9] P.X. Jiang, Y.J. Xu, J. Lv, R.F. Shi, S. He, J.D. Jackson, Experimental investigation of convection heat transfer of CO_2 at super-critical pressures in vertical mini tubes and in porous media, Appl. Thermal Engrg. 24 (2004) 1255–1270.
[10] S.V. Patankar, A calculation procedure for two-dimensional elliptic situation, Numer. Heat Transfer 4 (1981) 409–425.
[11] B.E. Launder, B.I. Sharma, Application of the energy-dissipation model of turbulence to the calculations of flow near a spinning disc, Lett. Heat Mass Transfer 1 (1974) 131–138.
[12] K.Y. Chien, Predictions of channel and boundary-layer flows with a low Reynolds number turbulence model, AIAA J. 23 (1982) 33–38.
[13] C.K.G. Lam, K. Bremhorst, A modified form of the k–ε model for predicting wall turbulence, ASME Trans. J. Fluids Engrg. 103 (1981) 456–460.
[14] K. Abe, T. Kondoh, Y. Nagano, A new turbulence model for predicting fluid flow and heat transfer in separating and reattaching flows—I. Flow field calculations, Internat. J. Heat Mass Transfer 37 (1994) 139–151.
[15] S. He, W.S. Kim, P.X. Jiang, J.D. Jackson, Simulation of mixed convection heat transfer to carbon dioxide at supercritical pressure, J. Mech. Engrg. Sci. 218 (2004) 1281–1296.
[16] S. He, P. An, J. Li, J.D. Jackson, Combined heat and mass transfer in a uniformly heated vertical tube with water film cooling, Internat. J. Heat Fluid Flow 19 (1998) 401–417.
[17] H. Herwig, O. Hausner, Critical view on new results in micro-fluid mechanics: an example, Internat. J. Heat Mass Transfer 46 (2003) 935–937.
[18] J.D. Jackson, W.B. Hall, Influences of buoyancy on heat transfer to fluids flowing in vertical tubes under turbulent conditions, in: Advanced Study Institute Book: Turbulent Forced Convection in Channels and Rod Bundles—Theory and Applications to Heat Exchangers and Reactors 2 (1979) 613–640.
[19] J.D. Jackson, Some striking features of heat transfer with fluids at pressures and temperatures near the critical point, in: Keynote paper for Int. Conf. on Energy Conversion & Application, ICECA, 2001, Wuhan, China.
[20] C.A. Bankston, D.M. McEligot, Turbulent and laminar heat transfer to gases with varying properties in the entry region of circular ducts, Internat. J. Heat Mass Transfer 13 (1970) 319–344.
[21] S.L. Kline, W.C. Reynolds, F.A. Schraub, P.W. Rundstadler, The structure of turbulent boundary layers, J. Fluid Mech. 30 (1966) 741–773.
[22] D.M. McEligot, C.W. Coon, H.C. Perkins, Relaminarisation in tubes, Internat. J. Heat Mass Transfer 13 (1970) 431–433.